metals

MDPI

Article

Atomistic Insights into the Competition between Damage and Dynamic Recrystallization Stimulated by the Precipitate $Mg_{17}Al_{12}$ in Magnesium Alloys

Yan Tang, Chao Xie *, Jianbin Chen and Xiaofeng Wang

Faculty of Mechanical Engineering and Mechanics, Ningbo University, Ningbo 315211, China; 1911081009@nbu.edu.cn (Y.T.); chenjianbin@nbu.edu.cn (J.C.); wangxiaofeng@nbu.edu.cn (X.W.)
* Correspondence: xiechao@nbu.edu.cn

Abstract: Precipitates are closely related to ductile damage and dynamic recrystallization (DRX) in magnesium alloys. Using molecular dynamics simulation and the embedded atomic method, the competition between damage and DRX stimulated by the precipitate of magnesium alloys is investigated. The effects of precipitate distribution and dimensions on the void nucleation, dislocation emission, void growth, and DRX of magnesium alloys are quantitatively discussed. It is found that compared to the system with a pre-existing void, the system with a single precipitate has two extra stages during damage evolution, namely atomic disorder and void nucleation, and its strength is clearly better. Void growth is attributed to the dislocation emission from void tips. Keeping the same volume fraction and varying the dimensions and spacings of the precipitates, the results show that the refinement and densification can increase the deformation compatibility of the system, hindering void nucleation and elevating the toughness. This can be attributed to the reduction in stress concentration and the prevalence of the particle-stimulated DRX.

Keywords: Mg alloy; precipitate; damage evolution; recrystallization; atomistic simulation

check for updates

Citation: Tang, Y.; Xie, C.; Chen, J.; Wang, X. Atomistic Insights into the Competition between Damage and Dynamic Recrystallization Stimulated by the Precipitate $Mg_{17}Al_{12}$ in Magnesium Alloys. *Metals* **2022**, *12*, 633. https://doi.org/10.3390/met12040633

Academic Editor: Ron Armstrong

Received: 13 March 2022
Accepted: 3 April 2022
Published: 7 April 2022

Publisher's Note: MDPI stays neutral with regard to jurisdictional claims in published maps and institutional affiliations.

Copyright: © 2022 by the authors. Licensee MDPI, Basel, Switzerland. This article is an open access article distributed under the terms and conditions of the Creative Commons Attribution (CC BY) license (https://creativecommons.org/licenses/by/4.0/).

1. Introduction

Magnesium alloys have received widespread attention in the automotive and aerospace fields due to their low densities and high specific strengths (strength-to-weight ratio) [1]. Compared with the common structural metals (such as aluminum and steel), magnesium alloys possess a lower plasticity and fracture toughness that limit their wide application in industrial fields. The low plasticity originates from the insufficient independent slip systems and the weak deformation compatibility of twinning and grain boundaries in the hexagonal close-packed (HCP) structure. In addition, the low fracture toughness is closely related to the limited dissipation of dislocation plastic energy near or at the crack tip [2].

Precipitation is an effective way to enhance the mechanical properties of magnesium alloys. The experiments in many previous studies found that the material ductility is related to the size of the precipitates [3–5]. In addition to strengthening [6–9], due to the deformation mismatch and stress concentration at the interfaces between precipitates and matrix, the particle-stimulated nucleation (PSN) that induces the generation of dynamic recrystallization (DRX) to accommodate plastic deformation is very common [10–13]. However, in the case that the plastic energy at the interfaces is not promptly dissipated by microstructures, the nucleation of voids at the interfaces or the rupture of precipitate itself might be driven. With increasing loading, the growth and coalescence of voids and cracks can lead to structural fracture and failure [10,14]. Therefore, the competition between DRX and damage is crucial for crystal toughness. The damage induced by precipitates is non-negligible for the design of Mg alloys. Some interesting studies have been reported. Horstemeyer et al. [15,16] developed a damage model describing the nucleation, growth, and coalescence of voids. They introduced the precipitate length parameter d and the

particle volume fraction f, gave the nucleation process of ductile damage induced by the precipitate based on the finite element method, and revealed the effect of the stress state on the void nucleation. Using digital image analysis, Lugo et al. [14] established a damage evolution model with the tensile strain as an internal variable and indicated that crack nucleation density increases exponentially with increasing strain and that the damage frequently occurs near the interface between the precipitate and the matrix. Kondori and Benzerga [17] experimentally reported that the fracture mode transits from quasi-brittle to ductile of the AZ31 magnesium alloy as the stress triaxiality decreases. The phenomenon was attributed to the transition of the damage micro-mechanisms from twinning-controlled fracture to microvoid coalescence fracture. The density of the precipitates affects the ductility of magnesium alloys. Fu et al. [18] experimentally found that the cracking of a massive number of precipitates in Mg-Gd alloy can greatly promote the formation of voids, leading to low ductility. Furthermore, the limited voids in the Mg-Gd-Zn-Zr alloy provide sufficient time and space for twinning, leading to good ductility. These studies on the damage evolution of magnesium alloy are based on phenomenological models and experiments and provide some important information on damage evolution. However, they neither fully capture the physical process of the damage evolution competing with DRX nor quantitatively explain the precipitate effect on the toughness.

Molecular dynamics (MD) is capable of tracing back to the atomic activities to quantitatively capture the activities and interactions among precipitates, dislocations, voids, grain boundaries, and so on. Jing et al. [19] simulated the evolution of nanovoids in the polycrystalline copper and indicated that the surface of the void with a larger diameter interacts with the surrounding grain boundaries, thereby promoting dislocation, emission, and void growth. In addition to damage, DRX has been investigated using MD. Liu et al. [20] studied the microstructure evolution of polycrystal copper under high strain rate loading. It revealed that the dislocation motion forms sub-grain boundaries, and sub-grains transform into refined grains via DRX. Rojas et al. [21] found that face-centered cubic particles can stimulate DRX, because dislocation emission and interaction forms the dislocation network under high-velocity impact, generating new grains. However, the transition from damage to DRX stimulated by particles, which is closely related to the crystal toughness, is still unclear.

The main alloying element in most Mg alloys is aluminum, which results in several precipitates. The most common one is the plate-shaped $Mg_{17}Al_{12}$ [4,22,23]. The purpose of the current paper is to atomistically study the competition between damage and DRX stimulated by the precipitate $Mg_{17}Al_{12}$ of magnesium alloys.

2. Methodology

In previous studies on the deformation behaviors of magnesium alloys, two potential functions, the embedded atom potential (EAM) and the modified embedded atom potential (MEAM), have been widely employed in atomic simulations. Considering the applicability, EAM [24] potential is applied in the current study.

Figure 1 shows the initial configuration of the single-crystal magnesium with a single plate-shaped precipitate $Mg_{17}Al_{12}$ lying on the basal plane [25,26]. The lattice constant of magnesium is a = 0.32 nm and c = 0.52 nm. The X, Y, and Z axes of the matrix are along the crystal directions $[10\bar{1}0]$, $[\bar{1}2\bar{1}0]$, and [0001], respectively. The periodic boundary condition is applied along the X, Y, and Z directions. The precipitate $Mg_{17}Al_{12}$ [27] with $[1\bar{1}1]$ a direction parallel to the Y axis of the magnesium possesses a volume fraction of 3%. The dimensions of the whole system with about 500,000 atoms are $21.3 \times 23.4 \times 22.9$ nm^3. A constant strain rate of 5×10^9/s along the z axis is applied [26,28,29]. The temperature of the thermostat atoms is controlled by a Nose–Hoover thermostat. Before loading, the system first performs energy minimization, and then relaxes to the lowest energy state through the NPT (constant number of particle (N), constant pressure (P) and constant temperature (T)) ensemble at a temperature of 300 K. The time step is 1 fs, and the temperature is controlled at 300 K during the tensile process.

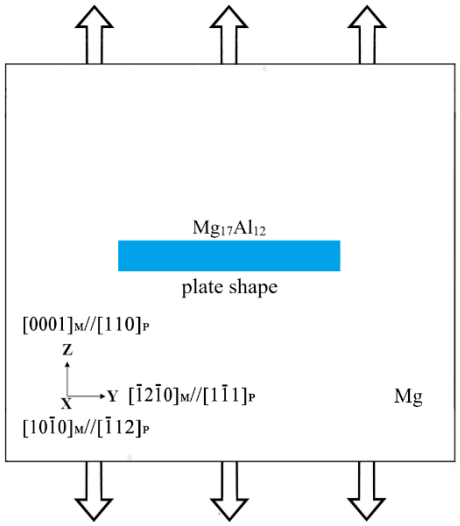


Figure 1. Initial schematic model of the single-crystal magnesium with a precipitate.

All simulations are performed by the Large-scale Atomic/Molecular Massively Parallel Simulator (LAMMPS) (14 May 2021, Sandia, NM, USA) [30]. The visualization tool OVITO (3.3.3, OVITO GmbH, Darmstadt, Germany) [31] is used to perform post-processing analyses. Common Neighbor Analysis [32] is used to distinguish crystal structures and lattice defects. Dislocation Analysis [33] is used to study dislocation behavior. In addition, the Construct Surface Mesh [34] is used to calculate the free surface volume fraction generated in the system.

The uniaxial tensile process along the *Z*-axis of the single-crystal pure magnesium system is simulated to validate the simulation condition. The uniaxial stress–strain curves (Figure 2) are obtained. The slope of the elastic section (elastic modulus) is consistent with Tang's molecular dynamics study on the tensile single-crystal pure magnesium [35]. The simulation condition is applicable for the current study.

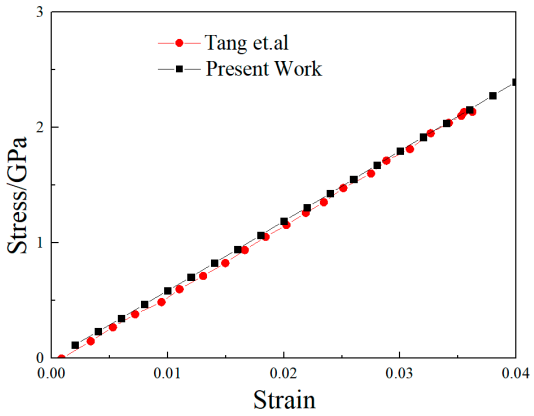


Figure 2. Stress vs. strain relationship of single-crystal pure magnesium stretched along the *Z*-axis.

3. Results

3.1. Single Crystal with a Single $Mg_{17}Al_{12}$

The damage evolution process of the single-crystal system with a single $Mg_{17}Al_{12}$ under uniaxial tension is first studied. The free surface fraction–strain curve is used to characterize the formation and growth of the free surface. The stress–strain curve is used to express the elastoplastic deformation and void nucleation–growth process of the system.

Figure 3 shows the variations in the uniaxial tensile stress and free surface fraction with the strain of the single-crystal with a single precipitate. Based on the features of the void volume–fraction curve [28], the damage evolution can be divided into four stages.

The atomic slices with the thickness of 10 Å, which are colored according to the magnitude of the potential energy and correspond to the 6 strains on the surface fraction–strain curve, are also presented in Figure 3.

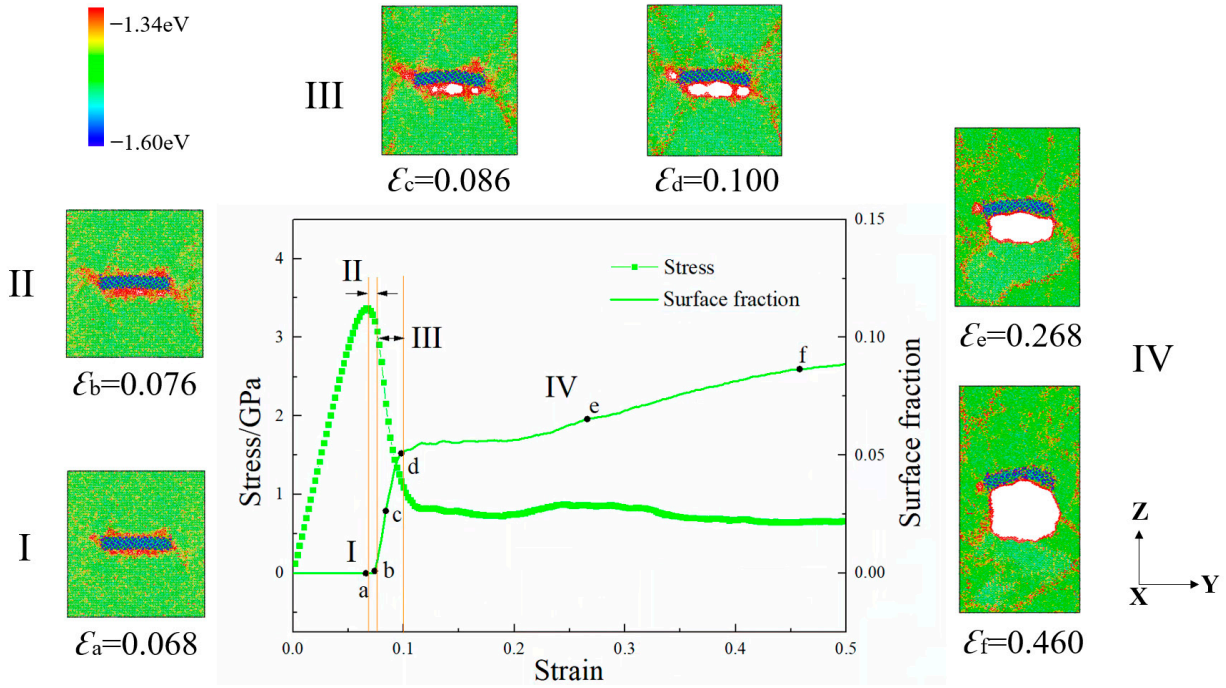


Figure 3. Stress vs. strain and free surface fraction vs. strain relationships of a single-crystal system with a single $Mg_{17}Al_{12}$ during tensile process.

Stage I: atomic disorder ($0.068 \geq \varepsilon \geq 0$). It can be seen from the potential energy diagram at strain a in Figure 3 that the potential energy around the precipitate is relatively higher, the atoms deviate from the original positions in the HCP structure and appear with local disorder, and a few tiny vacancies form. As the precipitate $Mg_{17}Al_{12}$ unit cell is a body-centered cubic crystal structure [22], the incoherent interface between the precipitate and matrix has the relatively higher interface energy [36,37]. Within this stage, the stress significantly increases, and the free surface volume fraction is not increased.

Stage II: void nucleation ($0.076 \geq \varepsilon > 0.068$). As shown in the potential energy diagram at strain b in Figure 3, the atoms clearly move, and the void nucleates at the interface below the precipitate. Within this stage, owing to the nucleation of voids, the stress begins to decrease; however, the free surface volume fraction still presents an insignificant elevation.

Stage III: lateral growth of the void ($0.100 \geq \varepsilon > 0.076$). As shown in the potential energy diagrams at strains c and d in Figure 3, the nucleated voids begin to grow along the basal plane where the interface between the precipitates and the matrix with the high potential energy is. Within this stage, the free surface volume fraction increases dramatically, the stress is quickly relaxed, and the energy of the system is released by the growth of the voids.

Stage IV: vertical growth of the void ($0.500 \geq \varepsilon > 0.100$). As shown in the potential energy diagrams at points e and f in Figure 3, when the voids begin to grow vertically, the growth rate of the free surface volume fraction begins to slow down. Within this stage, the stress enters the plateau.

Figure 4 shows the dislocation density variation and free surface evolution with strain. Atomic disorder within stage I has few dislocations, and the Burgers vectors mainly include $1/3<1\bar{1}00>$, $1/9<\bar{1}103>$, and $1/6<\bar{2}023>$. As the strain increases, the dislocation density increases within stage II, and the Burgers vectors $1/9<\bar{2}023>$ and $1/9<\bar{2}02\bar{3}>$ are newly emitted and accompanied by the nucleated voids. Within stage III, the uneven potential energy around the precipitate drives remarkable dislocation emission from the voids, which

is the major cause for stress relaxation [38]. Within this stage, the deformation switches from elasticity to elastoplasticity. Within stage IV, the free surface growth rate is slower than that in stage III, and the dislocation density drops off. The dislocation network (strain c and d in Figure 4) forms sub-boundaries, and the sub-boundaries migrate to form grain boundaries, leading to the DRX (shown in Figure 5).

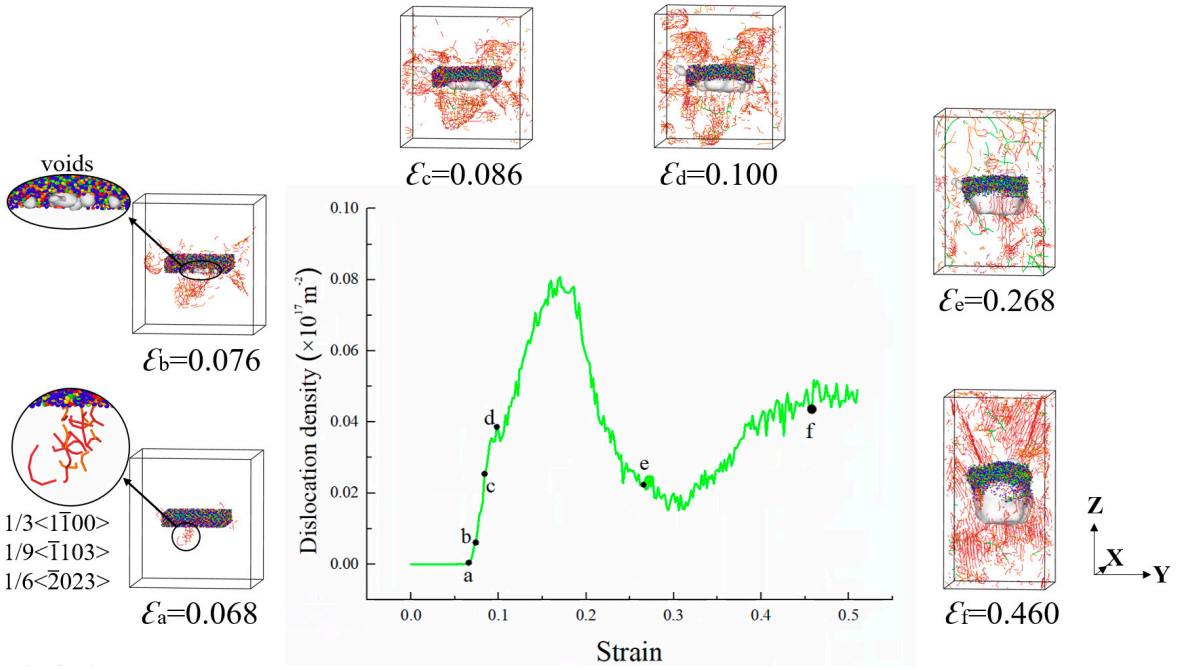


Figure 4. Dislocation density variation and free surface evolution with strain of a single-crystal system with a precipitate during tensile process (the internal white clouds represent voids).

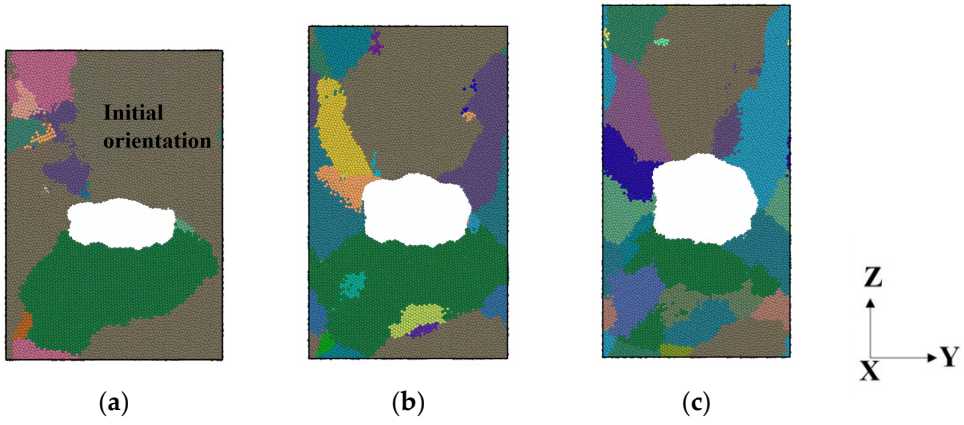


Figure 5. Atomic slices of the system with 1 precipitate in stage IV, (colored according to different orientations; gray represents the initial orientation) (**a**) at strain 0.268; (**b**) at strain 0.390; (**c**) at strain 0.460.

3.2. Single Crystal with a Void

A predefined void model is established by removing the precipitate from the system with a precipitate $Mg_{17}Al_{12}$. Figure 6 displays four snapshots of the void growth in the void system. In the beginning (strain 0.006), the predefined void does not apparently deform and no slip exists. Then (strain 0.046), the dislocations with the Burgers vectors 1/9<01$\bar{1}\bar{3}$> nucleate along <10$\bar{1}$2> direction near the tip of the void. With increasing strain (strain 0.050), in addition to the dilatation along the tensile direction, the dislocations with the Burgers vectors 1/3<10$\bar{1}$0>, 1/6<20$\bar{2}\bar{3}$>, 1/9<0$\bar{2}$23>, and 1/9<01$\bar{1}\bar{3}$> are emitted

from the tip, and therefore, the void starts to grow. As the strain reaches 0.118, more dislocations with the Burgers vectors 1/9<20$\bar{2}\bar{3}$> are emitted, significantly extending the void. The damage process of the void system does not include the atomic disorder and void nucleation stages, which is different from the single-crystal system with a precipitate.

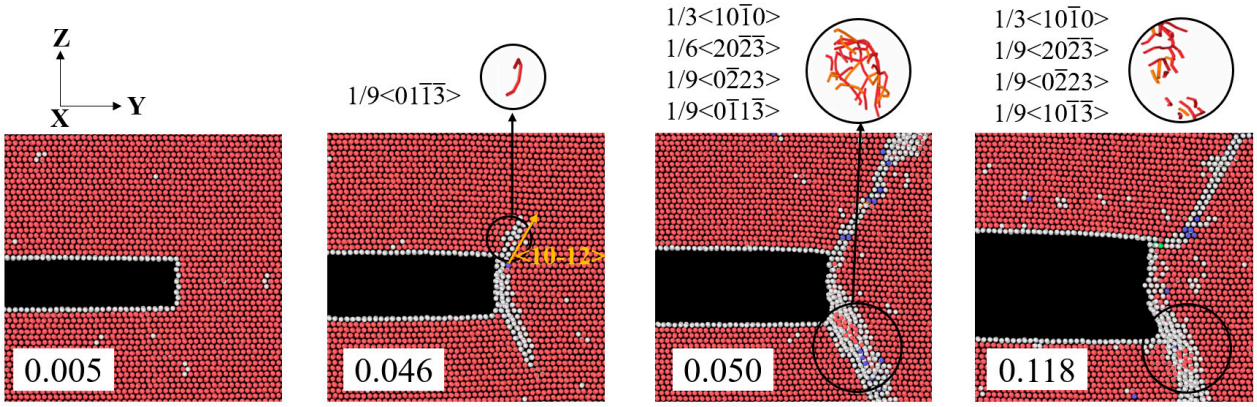


Figure 6. Void growth accompanied by dislocation emission in the void system.

The ultimate stresses and the growth of the void of the systems with a single precipitate, a single void, and no defects are compared in Figure 7. Since the void itself is introduced as a defect, the ultimate stress is naturally the lowest. Moreover, the void, without the atomic disorder and the void nucleation stages, clearly grows faster. Due to the high energy at the interface between the precipitate and matrix, the void easily nucleates at the interface, and the plasticity of the system with a single precipitate is worse than that of the pure magnesium system. The ultimate stress of the precipitate system is slightly lower than that of the pure magnesium system, which is not contradictory to the precipitate strengthening mechanism in the systems with multiple defects. To the authors' best knowledge, the ultimate stress in the single-crystal pure magnesium system with no defects is close to the theoretical value, and it is naturally higher than that of the system with a precipitate.

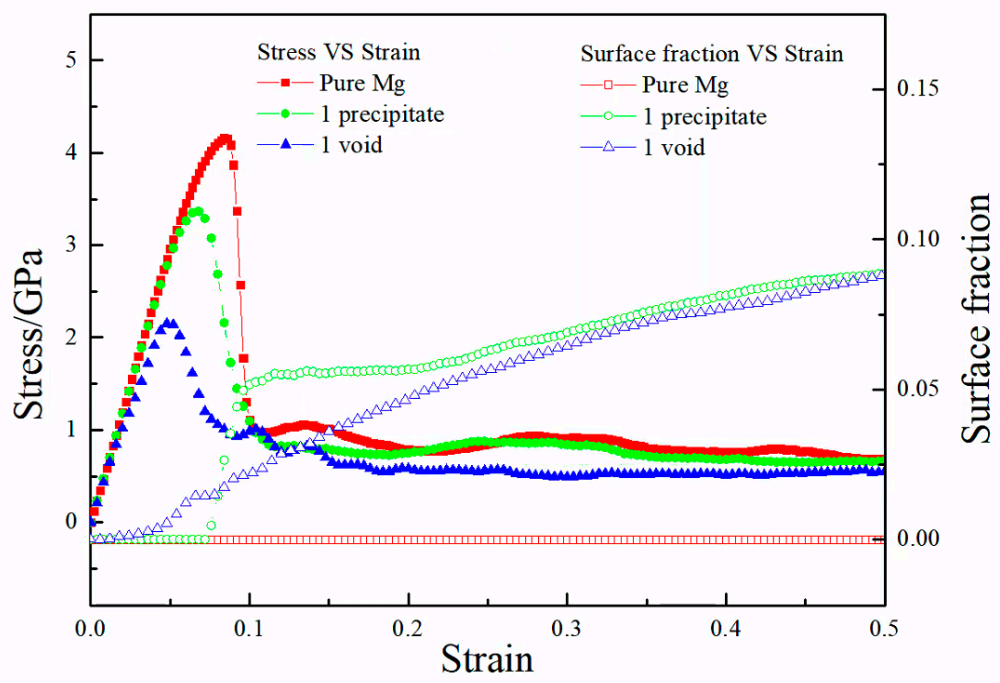
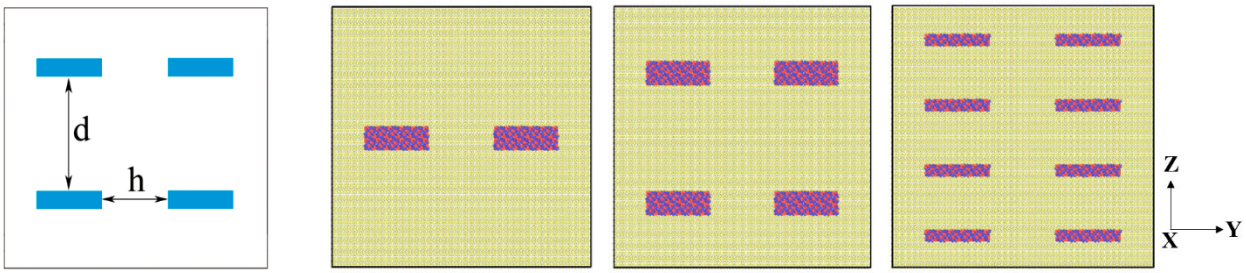


Figure 7. Comparisons of ultimate stress and free surface fraction growth among the three systems.

3.3. Single-Crystal with Multiple Precipitates

Keeping the same volume fraction of the precipitate $Mg_{17}Al_{12}$ and varying the dimensions and spacings (d, h) of the precipitates (Figure 8a), the effect of the precipitate distribution on the ultimate stress and the growth of the free surface is analyzed. As shown in Figure 8b, the single precipitate is refined into 2, 4, and 8 equal parts placed periodically in the magnesium matrix.



(**a**) (**b**)

Figure 8. The cross sections of systems. (**a**) Schematic diagrams; (**b**) The systems with 2, 4, and 8 precipitates.

Stress vs. strain and the surface fraction vs. strain relationships of the single-crystal pure magnesium system and the precipitate systems with different dimensions and spacings are shown in Figure 9. The ultimate stresses of the precipitate systems are lower than that of the single-crystal pure magnesium system. There is no significant difference in the ultimate stress of the precipitate system. However, the free surface fractions of the system with a precipitate grows faster than that of the system with 2 precipitates. With the refinement and densification, the systems with 4 and 8 precipitates have no free surface, which indicates that no voids are formed. The specific microstructure evolution of these systems is clarified as follows.

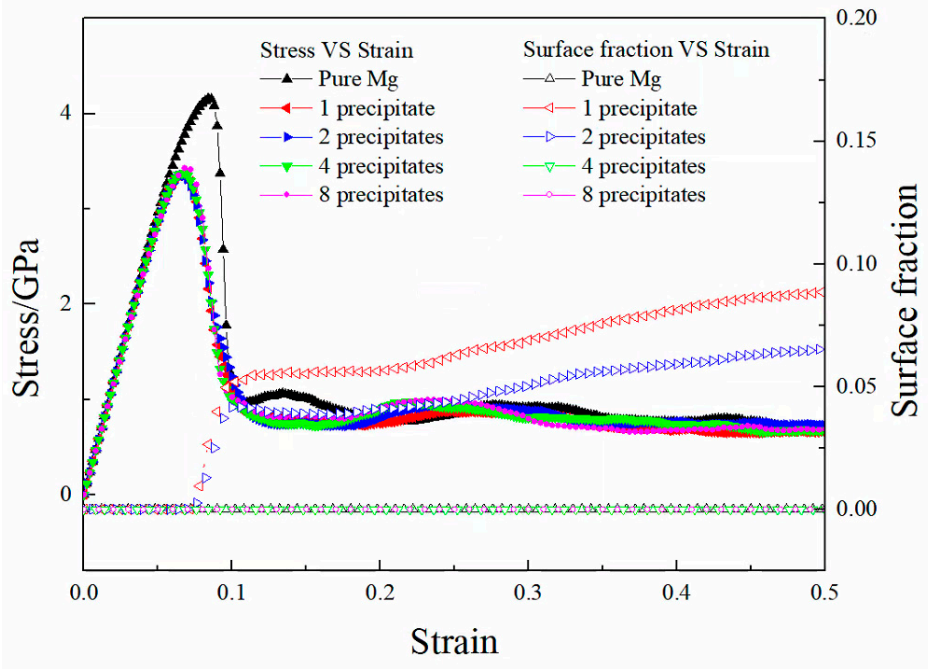


Figure 9. Stress vs. strain and surface fraction vs. strain relationships of multiple systems.

Figure 10a shows the potential energy cross sections together with the void and dislocation evolution of the system with two precipitates. Because the incoherent interfaces between the precipitates and matrix possess a higher interface energy (strain a), the atoms

at the interfaces are inclined to be driven to move. Therefore, the dislocations preferentially nucleate around the precipitate (strain b), and the voids gradually grow (strain c, d). Then (strain e), the dislocation density also decreases because of the DRX. Finally, driven by the back stress due to the growth of the voids, the precipitates deflect by a small angle [39–42] (strain f).

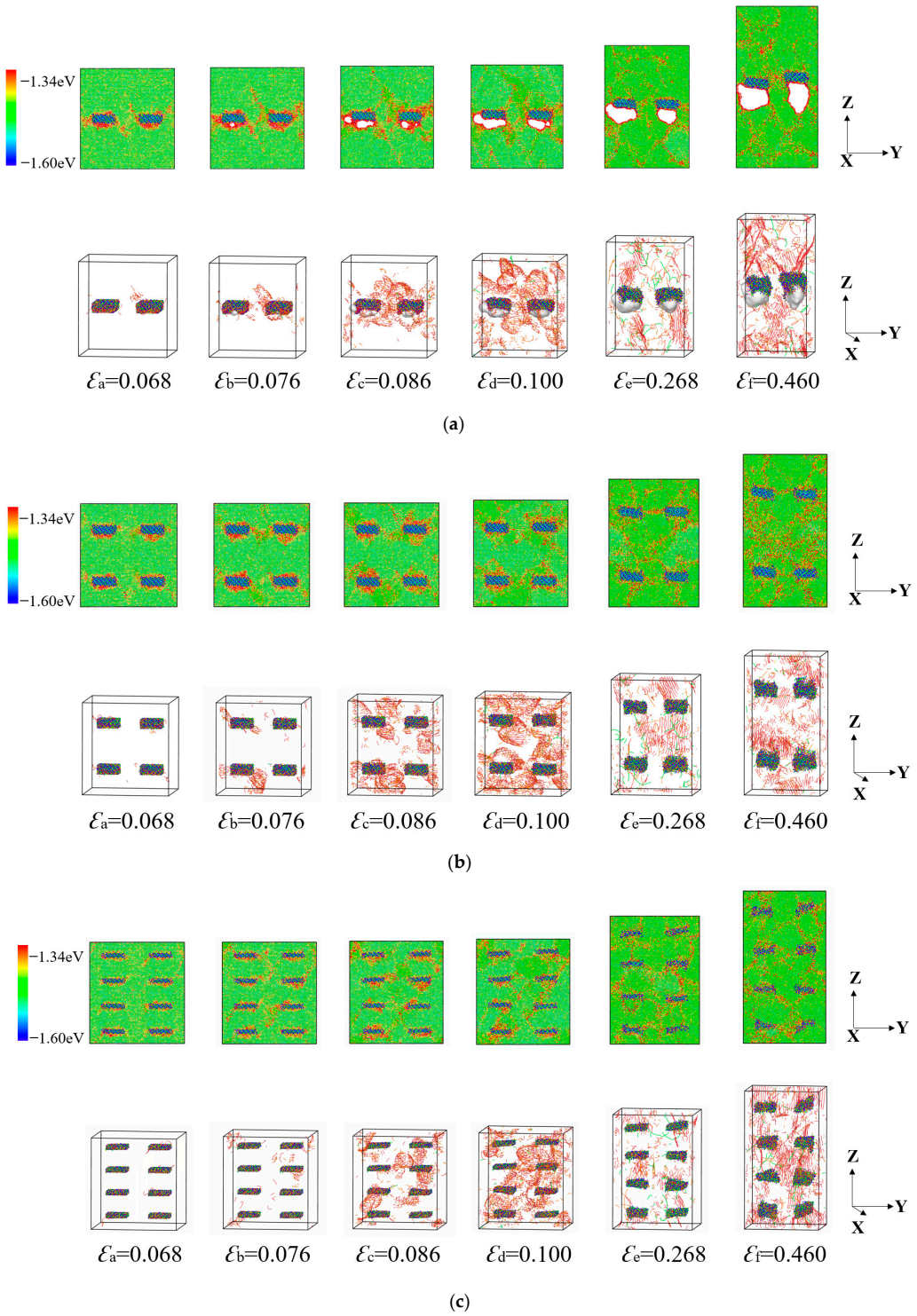


Figure 10. Potential energy cross-section, void, and dislocation evolution diagrams of the systems with multiple precipitates: (**a**) 2 precipitates; (**b**) 4 precipitates; (**c**) 8 precipitates.

For the systems with 4 and 8 precipitates shown in Figure 10b,c, the microstructure evolution process becomes different compared to the others. Unlike the systems with 1 and 2 precipitates, although dislocations around the precipitates are still active, the voids do not nucleate at the interfaces anymore.

4. Discussion

By analyzing the local lattice orientation (Figure 11), it can be observed that the above systems form different orientations in tensile processes, developing DRX stimulated by precipitates. The systems with 4 and 8 precipitates present more DRX at strain 0.268 (Figure 11a). The DRX mechanism softens the local orientation under the temperature and mechanical loading. Therefore, the stress–strain curves of the 1 and 2 precipitate systems have the plateau, and the voids do not coalesce rapidly (strain e and f in Figure 3), while the 4 and 8 precipitates systems provide more sites for DRX, resulting in softening without the void. The refinement and densification of the precipitates favor DRX rather than damage, which is consistent with the experimental results [12,43,44].

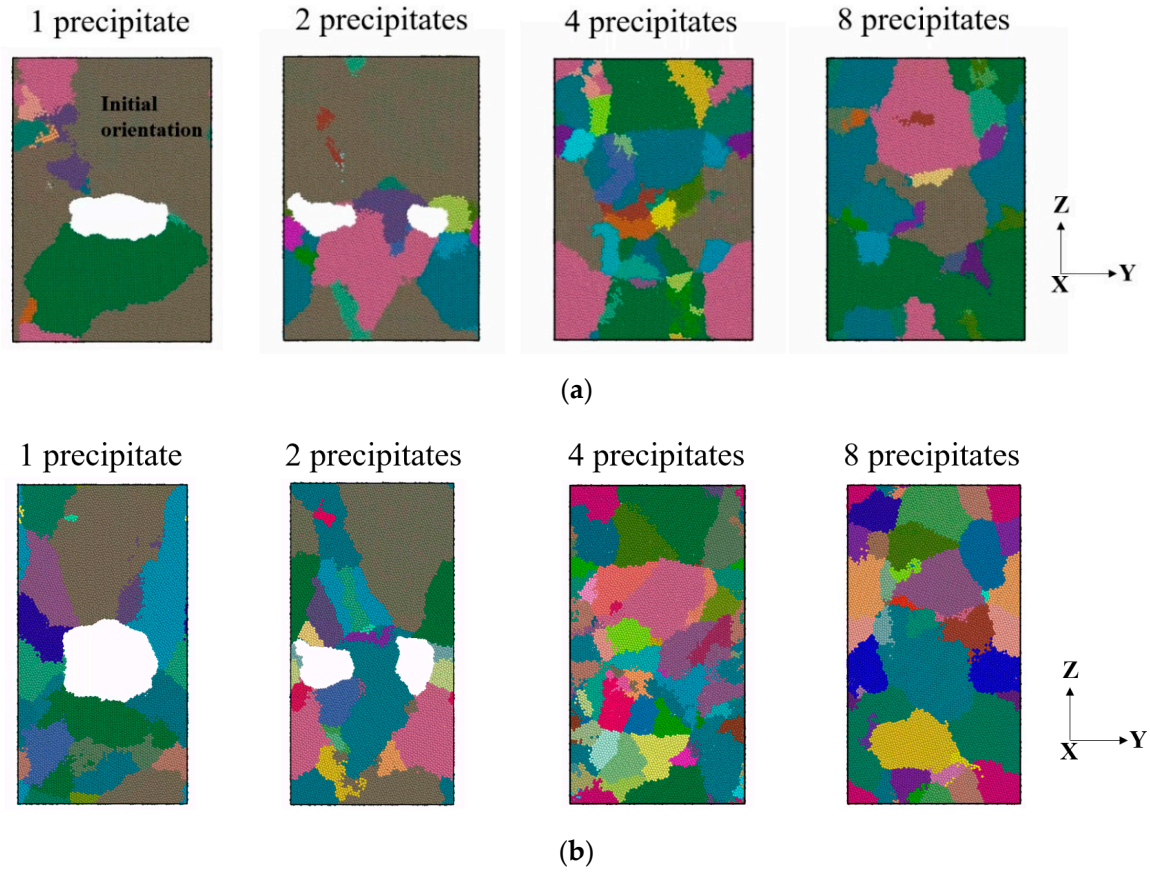


Figure 11. Atomic slices of the system with 1, 2, 4, and 8 precipitates (**a**) at strain 0.268 (**b**) at strain 0.460.

In addition, the contours of the shear stress components σ_{zy} and σ_{zx} at strain 0.068 reveal the stress concentration around the precipitates (Figure 12). The larger precipitate leads to the greater shear stresses. The mismatch between the larger precipitate and matrix induces the higher stress concentration at the interface, which drives not only the nucleation of dislocations but also the nucleation of voids. Conversely, the fine and dense precipitates possess the weaker stress concentrations that can be relaxed only by dislocation nucleation. The dimension and spacing of the precipitate determine the competition between damage and DRX.

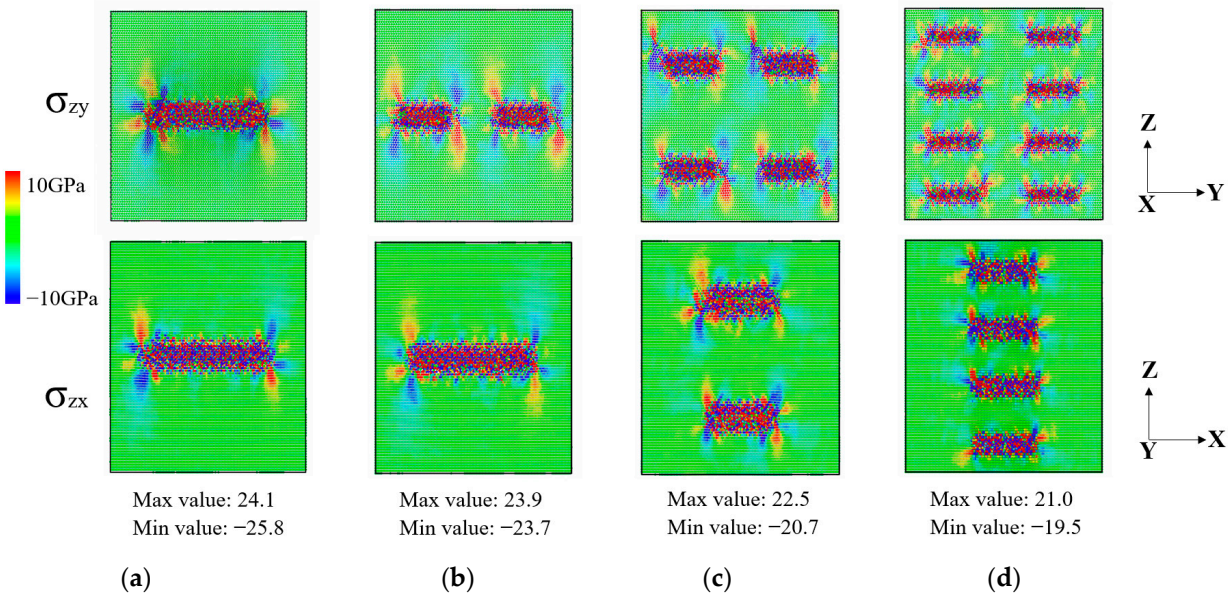


Figure 12. Contours of stress components at strain 0.068 (the top is σ_{zy}, the bottom is σ_{zx}) (**a**) 1 precipitate; (**b**) 2 precipitates; (**c**) 4 precipitates; (**d**) 8 precipitates.

5. Conclusions

In the current study, the MD simulation is utilized to investigate the competition between damage and DRX induced by the precipitate $Mg_{17}Al_{12}$ in magnesium alloys. The influences of the precipitate dimensions and spacings on the void nucleation, dislocation emission, void growth, and DRX of the single-crystal magnesium system are analyzed. The toughening mechanism is discussed. Some conclusions can be drawn as follows:

(1) The incoherent interfaces between the precipitates and the matrix, with the high interfacial energy, are capable of motivating atomic disorder and void nucleation. The formed voids can grow faster due to $1/3<10\bar{1}0>$, $1/9<0\bar{2}23>$, $1/9<20\bar{2}3>$, and $1/9<10\bar{1}3>$ dislocation emission from void tips under large deformations.

(2) The coarse and sparse precipitates are inclined to promote the nucleation and growth of voids at the interfaces. When the precipitates are fine and dense, it is difficult to generate voids at the interfaces due to the reduction in stress concentration. In addition, more precipitates, such as the embryo sites, can stimulate more DRX to coordinate the stresses and deformations. Therefore, the dimension and space of precipitates dominate the competition between damage and DRX, and the refinement and densification of precipitates can significantly enhance crystal toughness.

Author Contributions: Conceptualization, C.X.; Methodology, C.X. and Y.T.; Software, Y.T. and X.W.; Validation, J.C.; Data curation, Y.T.; Supervision, C.X.; Writing—original draft preparation, Y.T.; Writing—review and editing, C.X. and J.C. All authors have read and agreed to the published version of the manuscript.

Funding: This research was funded by the National Natural Science Foundation of China (No. 11872216), the Zhejiang Provincial Natural Science Foundation of China (No. Y22A021168), the Natural Sci-ence Foundation of Ningbo City (No. 202003N4083), and the Ningbo Science and Technology Major Project (Grant No. 2022Z002).

Institutional Review Board Statement: Not applicable.

Informed Consent Statement: Not applicable.

Data Availability Statement: Data available on request.

Conflicts of Interest: The authors declare no conflict of interest.

References

1. Wang, Y.; Xie, C.; Fang, Q.; Liu, X.; Zhang, M.; Liu, Y.; Li, L. Toughening effect of the nanoscale twinning induced by particle/matrix interfacial fracture on fine-grained Mg alloys. *Int. J. Solids Struct.* **2016**, *102–103*, 230–237. [CrossRef]
2. Wu, Z.; Curtin, W.A. Brittle and ductile crack-tip behavior in magnesium. *Acta Mater.* **2015**, *88*, 1–12. [CrossRef]
3. Peng, H.; Hu, L.; Li, L.; Zhang, W. Ripening of $L1_2$ nanoparticles and their effects on mechanical properties of $Ni_{28}Co_{28}Fe_{21}Cr_{15}A_{l4}Ti_4$ high-entropy alloys. *Mater. Sci. Eng. A* **2019**, *772*, 138803. [CrossRef]
4. Ming, K.; Bi, X.; Wang, J. Realizing strength-ductility combination of coarse-grained $Al_{0.2}Co_{1.5}CrFeNi_{1.5}Ti_{0.3}$ alloy via nano-sized, coherent precipitates. *Int. J. Plast.* **2018**, *100*, 177–191. [CrossRef]
5. Xu, S.S.; Zhao, Y.; Chen, D.; Sun, L.W.; Chen, L.; Tong, X.; Liu, C.T.; Zhang, Z.W. Nanoscale precipitation and its influence on strengthening mechanisms in an ultra-high strength low-carbon steel. *Int. J. Plast.* **2019**, *113*, 99–110. [CrossRef]
6. Fan, H.; Ngan, A.H.; Gan, K.; El-Awady, J.A. Origin of double-peak precipitation hardening in metallic alloys. *Int. J. Plast.* **2018**, *111*, 152–167. [CrossRef]
7. Nie, J. Effects of precipitate shape and orientation on dispersion strengthening in magnesium alloys. *Scr. Mater.* **2003**, *48*, 1009–1015. [CrossRef]
8. Hidalgo-Manrique, P.; Robson, J.; Perez-Prado, M.T. Precipitation strengthening and reversed yield stress asymmetry in Mg alloys containing rare-earth elements: A quantitative study. *Acta Mater.* **2016**, *124*, 456–467. [CrossRef]
9. Toda-Caraballo, I.; Galindo-Nava, E.I.; Rivera-Díaz-Del-Castillo, P.E. Understanding the factors influencing yield strength on Mg alloys. *Acta Mater.* **2014**, *75*, 287–296. [CrossRef]
10. Humphreys, F. The nucleation of recrystallization at second phase particles in deformed aluminium. *Acta Met.* **1977**, *25*, 1323–1344. [CrossRef]
11. Wang, X.J.; Hu, X.S.; Nie, K.B.; Deng, K.K.; Wu, K.; Zheng, M.Y. Dynamic recrystallization behavior of particle reinforced Mg matrix composites fabri-cated by stir casting. *Mater. Sci. Eng. A* **2012**, *545*, 38–43. [CrossRef]
12. Robson, J.; Henry, D.; Davis, B. Particle effects on recrystallization in magnesium–manganese alloys: Particle-stimulated nucleation. *Acta Mater.* **2009**, *57*, 2739–2747. [CrossRef]
13. Kim, H.J.; Jin, S.-C.; Jung, J.-G.; Park, S.H. Influence of undissolved second-phase particles on dynamic recrystallization behavior of Mg–7Sn–1Al–1Zn alloy during low- and high-temperature extrusions. *J. Mater. Sci. Technol.* **2020**, *71*, 87–97. [CrossRef]
14. Lugo, M.; Tschopp, M.; Jordon, J.; Horstemeyer, M. Microstructure and damage evolution during tensile loading in a wrought magnesium alloy. *Scr. Mater.* **2011**, *64*, 912–915. [CrossRef]
15. Horstemeyer, M.F.; Lathrop, J.; Gokhale, A.M.; Dighe, M. Modeling stress state dependent damage evolution in a cast Al–Si–Mg aluminum alloy. *Theor. Appl. Fract. Mech.* **2000**, *33*, 31–47. [CrossRef]
16. Horstemeyer, M.F.; Gokhale, A.M. A void–crack nucleation model for ductile metals. *Int. J. Solids Struct.* **1999**, *36*, 5029–5055. [CrossRef]
17. Kondori, B.; Benzerga, A.A. Effect of Stress Triaxiality on the Flow and Fracture of Mg Alloy AZ_{31}. *Met. Mater. Trans. A* **2014**, *45*, 3292–3307. [CrossRef]
18. Fu, W.; Wang, R.; Zhang, J.; Wu, K.; Liu, G.; Sun, J. The effect of precipitates on voiding, twinning, and fracture behaviors in Mg alloys. *Mater. Sci. Eng. A* **2018**, *720*, 98–109. [CrossRef]
19. Jing, P.; Yuan, L.; Shivpuri, R.; Xu, C.; Zhang, Y.; Shan, D.; Guo, B. Evolution of spherical nanovoids within copper polycrystals during plastic straining: Atomistic investigation. *Int. J. Plast.* **2017**, *100*, 122–141. [CrossRef]
20. Liu, H.; Zhang, Y.; Ma, Y.; Cui, J.; Li, M.; Gong, J.; Wang, X. Molecular dynamics simulation of nanostructure formation in copper foil under laser shock forming. *Comput. Mater. Sci.* **2019**, *172*, 109352. [CrossRef]
21. Rojas, D.F.; Isiet, M.; Ponga, M. Dynamic recrystallization in face-centered cubic particles during high-velocity impacts. *Mech. Mater.* **2022**, *168*, 104268. [CrossRef]
22. Polmear I, J. Magnesium alloys and applications. *Mater. Sci. Tech.* **1994**, *10*, 1–16. [CrossRef]
23. Wang, N.; Yu, W.-Y.; Tang, B.-Y.; Peng, L.-M.; Ding, W.-J. Structural and mechanical properties of $Mg_{17}Al_{12}$and $Mg_{24}Y_5$from first-principles calculations. *J. Phys. D Appl. Phys.* **2008**, *41*, 195408. [CrossRef]
24. Liu, X.-Y.; Ohotnicky, P.; Adams, J.; Rohrer, C.; Hyland, R. Anisotropic surface segregation in Al-Mg alloys. *Surf. Sci.* **1997**, *373*, 357–370. [CrossRef]
25. Xie, C.; Xiang, M.; Zhang, Z.; Liu, X.; Zhu, B.; Chen, J.; Wang, X.; Shu, X.; Fang, Q. Effect of local stresses of primary twinning on double twinning, twin intersection and their competition. *Mater. Sci. Eng. A* **2019**, *769*, 138498. [CrossRef]
26. Zhou, Y.; Yang, Z.; Lu, Z. Dynamic crack propagation in copper bicrystals grain boundary by atomistic simulation. *Mater. Sci. Eng. A* **2014**, *599*, 116–124. [CrossRef]
27. Zhang, M.-X.; Kelly, P. Crystallography of $Mg_{17}Al_{12}$ precipitates in $AZ_{91}D$ alloy. *Scr. Mater.* **2003**, *48*, 647–652. [CrossRef]
28. Yang, X.; Zeng, X.; Wang, J.; Wang, F.; Ding, J. Atomic-scale modeling of the void nucleation, growth, and coalescence in Al at high strain rates. *Mech. Mater.* **2019**, *135*, 98–113. [CrossRef]
29. Huang, M.; Yang, X.; Chen, G.; Li, G.; Zhai, P. Molecular dynamics simulations of the effects of nanopores on mechanical behavior in the Mg_2Sn system. *Comput. Mater. Sci.* **2019**, *161*, 177–189. [CrossRef]
30. Plimpton, S. Fast parallel algorithms for short-range molecular dynamics. *J. Comput. Phys.* **1995**, *117*, 1–19. [CrossRef]
31. Stukowski, A. Visualization and analysis of atomistic simulation data with OVITO—The Open Visualization Tool. *Model. Simul. Mater. Sci. Eng.* **2009**, *18*, 015012. [CrossRef]

32. Faken, D.; Jónsson, H. Systematic analysis of local atomic structure combined with 3D computer graphics. *Comput. Mater. Sci.* **1994**, *2*, 279–286. [CrossRef]
33. Stukowski, A.; Bulatov, V.V.; Arsenlis, A. Automated identification and indexing of dislocations in crystal interfaces. *Model. Simul. Mater. Sci. Eng.* **2012**, *20*, 085007. [CrossRef]
34. Stukowski, A. Computational analysis methods in atomistic modeling of crystals. *JOM* **2013**, *66*, 399–407. [CrossRef]
35. Tang, T.; Kim, S.; Horstemeyer, M. Molecular dynamics simulations of void growth and coalescence in single crystal magnesium. *Acta Mater.* **2010**, *58*, 4742–4759. [CrossRef]
36. Vaid, A.; Guénolé, J.; Prakash, A.; Korte-Kerzel, S.; Bitzek, E. Atomistic simulations of basal dislocations in Mg interacting with $Mg_{17}Al_{12}$ precip-itates. *Materialia* **2019**, *7*, 100355. [CrossRef]
37. Wang, R.; Eliezer, A.; Gutman, E. Microstructures and dislocations in the stressed AZ91D magnesium alloys. *Mater. Sci. Eng. A* **2003**, *344*, 279–287. [CrossRef]
38. Wen, Z.; Wang, J.; Wu, Y.; Zhou, K.; Yue, Z. Atomistic simulation analysis of the effects of void interaction on void growth and coalescence in a metallic system. *Curr. Appl. Phys.* **2018**, *18*, 744–751. [CrossRef]
39. Liu, F.; Xin, R.; Zhang, M.-X.; Pérez-Prado, M.T.; Liu, Q. Evaluating the orientation relationship of prismatic precipitates generated by detwinning in Mg alloys. *Acta Mater.* **2020**, *195*, 263–273. [CrossRef]
40. Gharghouri, M.A.; Weatherly, G.C.; Embury, J.D. The interaction of twins and precipitates in a Mg-7.7 at.% Al alloy. *Philos. Mag. A* **1998**, *78*, 1137–1149. [CrossRef]
41. Wang, F.; Li, B. Origin of deflection of precipitates during interaction with a migrating twin boundary in magnesium alloys. *Comput. Mater. Sci.* **2018**, *154*, 472–480. [CrossRef]
42. Jain, J.; Cizek, P.; Poole, W.J.; Barnett, M.R. The role of back stress caused by precipitates on {101 2} twinning in a Mg–6Zn alloy. *Mater. Sci. Eng. A.* **2015**, *647*, 66–73. [CrossRef]
43. Jung, J.G.; Park, S.H.; Yu, H.; Kim, Y.M.; Lee, Y.K.; You, B.S. Improved mechanical properties of Mg–7.6 Al–0.4 Zn alloy through aging prior to extru-sion. *Scr. Mater.* **2014**, *93*, 8–11. [CrossRef]
44. Luo, L.; Xiao, Z.; Huo, Q.; Yang, Y.; Huang, W.; Guo, J.; Ye, Y.; Yang, X. Enhanced mechanical properties of a hot-extruded AZ80 Mg alloy rod by pre-treatments and post-hot compression. *J. Alloy. Compd.* **2018**, *740*, 180–193. [CrossRef]